Interfacial Phenomena and Heat Transfer, 3 (3): 221–229 (2015)

BEYOND TANNER'S LAW: ROLE OF CONTACT LINE EVAPORATION ON THE SPREADING OF VISCOUS DROPLET

W. Bou-Zeid & D. Brutin*

Aix Marseille University, CNRS, IUSTI UMR 7343, 13013, Marseille, France

*Address all correspondence to: D. Brutin, E-mail: david.brutin@univ-amu.fr

The effect of relative humidity and viscosity on the spreading dynamics of water-glycerol mixtures was analyzed for a range of humidities from 20% to 80%. Droplets of identical volume were deposited on ultra-clean glass substrates. We demonstrated that, in addition to the competition between viscous forces, capillary forces, and disjoining pressure, droplet spreading was also affected by the evaporation that occurred at the triple line. We provide an updated Tanner's spreading law, which was modified to take into account the evaporative contribution. The same mechanism can be applied to adjust any fluid to Tanner's coefficient of 1/10.

KEY WORDS: *viscous drops, evaporation, wettability*

1. INTRODUCTION

The dynamics of the spreading/evaporation process of liquid drops is an important topic of interest because it plays a crucial role in many industrial and material operations. A few of these applications include printing, painting, coating, lubrication, and spraying (Attinger et al., 2000). One of the main problems in these applications remains the precise control of all relevant parameters for droplet spreading/evaporation processes. Substrate temperature and evaporation rate are examples of such parameters that strongly modify the spreading/evaporation dynamics (Chhasatia et al., 2010; Anderson and Davis, 1995).

When a liquid droplet contacts a wettable solid surface, the out-of-balance interfacial force $\gamma(\cos\theta_{\mathrm{eq}} - \cos\theta_D)$ drives the liquid to move in the direction of restoring equilibrium, whereas the inertia of the liquid drop, the friction at the contact line, and the viscous dissipation within the drop resist the spreading of the liquid (Bonn et al., 2009), where γ, θ_{eq}, and θ_D are the surface tension, the equilibrium, and dynamic contact angles, respectively. However, one commonly used method to analyze spreading dynamics is by matching the curves of the spreading radius r versus the spreading time t with a power law, $r(t) \sim t^n$, where n represents the spreading or wetting exponent. For a drop of complete wetting fluid ($\theta_{\mathrm{eq}} = 0$) with a radius much smaller than the capillary length, $l_c = \sqrt{\gamma/\rho g}$ (effect of gravity is negligible for Bond numbers much below 1), the drop spreads indefinitely, presumably until it reaches a film thickness controlled by the surface forces, where ρ is the drop density and g is the gravitational acceleration. Bond number is defined by the ratio of the drop diameter (D) squared by the capillary length squared ($\mathrm{Bo} = D^2/l_c^2$).

For viscous spreading of small droplets, the hydrodynamic theory predicts that the initial dynamic wetting is driven by capillarity and is opposed by viscous dissipation in the liquid wedgelike region near the contact line. By balancing the capillary and viscous forces, the radius r of spreading drops scales over time t according to the following power law, which is known as Tanner's law (Tanner, 1979): $r(t) \sim R(\gamma t/\mu R)^n$, where $n = 1/10$, R is the drop radius, and μ is the dynamic viscosity. This law can be simply obtained by considering that the shape of the drop is a thin spherical cap and that the dynamic contact angle θ_D is related to the contact line velocity using the Cox-Voinov relationship (Cox, 1986): $\theta_D^3 \sim \mathrm{Ca}$. Moreover, Tanner's law predicts the long-term spreading and does not apply at short time.

2169–2785/15/$35.00

NOMENCLATURE

μ	dynamic viscosity (Pa.s)	$r(t)$	wetted drop radius (m)
n	wetting exponent (also called Tanner's exponent)	ϱ	density (kg.m^{-3})
l_c	capillary length (m)	Ca	capillary number
s	surface tension (N.m^{-1})	V	drop volume (m^3)
g	earth gravity (m^2.s^{-1})	T	temperature (C)
Bo	Bond number	t	time (s)
D	drop diameter (m)	C	concentration (%)
θ	contact angle (deg)	RH	relative humidity (%)

As the wetting radius of the droplet grows beyond the capillary length (for centimetric-sized drops), gravity becomes the dominant spreading force and the shape of the drop becomes pancake-like, curved only at the drop rim, yielding a spreading exponent n = 1/8 when bulk phase fluid dissipation dominates or n = 1/7 when contact line fluid dissipation dominates (Lopez et al., 1976). A crossover between n = 1/10 and 1/8 was reported in the experiments of (Cazabat and Stuart, 1986), while Ehrhard (1993) found a crossover from 1/10 to 1/7.

For liquids of different viscosities, Duvivier et al. (2011) estimated the coefficient of contact line friction from the molecular kinetic theory, by fitting the experimental spreading radius $r(t)$ for drops with different viscosities. In their experiment, the authors showed that the contact-line friction of the liquid-air interface versus the glass is proportional to the viscosity and exponentially dependent on the work of adhesion. A departure from Tanner's law was reported by de Ruijter et al. (1999) and was attributed to a change in the physical mechanism by which the contact line advances across the solid surface. It has shown also that several kinetic regimes associated with different dissipation channels have to be considered, but they have a dominant effect on the kinetics of the wetting process at different time scales.

Most studies have focused on understanding the factors (viscosity, density, surface tension, drop volume, and surface wettability) that affect the spreading dynamics of pure liquids. These studies have been described in the literature based on the hydrodynamic theory (de Gennes, 1985; Cox, 1986). However, few experimental and theoretical studies have attempted to investigate the effect of the evaporation rate on the spreading dynamics of volatile liquids (Ajaev et al., 2010). Ajaev et al. (2010) found a deviations from Tanner's law when the interface shape changes rapidly in response to rapid changes of the heater temperature. In their work, the evaporation rate was modified by heating the substrate, whereas in our work we changed the relative humidity which is one of the easiest parameters to be controlled.

The spreading dynamics of viscous droplets has been investigated both experimentally and numerically (Roques-Carmes et al., 2010; Eddi et al., 2013; Legendre and Maglio, 2013). Roques-Carmes et al. (2010) performed experiments with droplets of different water-glycerol mixtures (V = 15 μl, μ = [20–1150] mPa.s). The authors showed that the wetting exponent corresponding to the first and second regimes increased with increasing viscosity, whereas the constant (pre-exponential factor) decreased in the first regime and increased in the second one. For drops of high viscosity ($\mu > 50$ mPa.s), the authors found a power law exponent close to that of Tanner's law. Eddi et al. (2013) performed experiments with droplets of different water-glycerol mixtures (μ=15 mPa.s, 50 mPa.s, 220 mPa.s, 1120 mPa.s) on glass substrate. The authors used a combined bottom and side-view camera (high-speed recording: 250 images/s) to investigate the early times of spreading just after the start of the process. In this work, the authors observed a scaling in the contact radius as $r(t) \sim t^n$ (1/5 $< n <$ 4/5) with a dependence on liquid viscosity. For four different viscosities, the authors experimentally showed that the dynamics behavior decreased with viscosity and that the cross-over appeared at an earlier time point and was sharper for lower viscosities. Legendre and Maglio (2013) performed numerical simulations to investigate the effect of the main parameters (viscosity, density, surface tension, drop volume, and surface wettability) that controlled the early spreading dynamics. For high viscous drops, the authors used a simplified force balance between the capillary pressure and the viscous stress near the contact line

($\gamma R_0/r^2 \sim \mu(dr/dt)/l$) and observed an increase in the spreading law from $t^{1/2}$ to $t^{2/3}$ according to Tanner's law $t^{1/10}$, where l is the characteristic length controlling the shear stress at the contact line.

The aim of our experimental work was to study the effect of the evaporation rate on spreading through the triple line dynamics for various concentrations of water-glycerol mixtures. This work was performed according to previous studies using whole human blood to better understand the physical mechanisms that govern the spreading of a drop of human blood (Bou-Zeid et al., 2013; Bou-Zeid and Brutin, 2014). However, we aimed to study a fluid model that has the same physical properties as whole human blood. Water-glycerol mixtures exhibit the same density and surface tension, and their viscosity can be altered by changing their concentration ratio.

2. EXPERIMENTAL SETUP

The spontaneous spreading of a sessile drop was investigated using the setup shown in Fig. 1. The spreading process was performed in a glove box (316 liters) under controlled atmospheric conditions (ambient temperature T_a = 23.0 $\pm$ 1.0°C, atmospheric pressure P_a = 998 $\pm$ 0.9 hPa). The volume of this box was sufficient to prevent saturation of the atmosphere with the vapor generated. The humidity levels inside the glovebox were controlled by supplying either dry or humid air, and a range of relative humidity (RH) values from 20% to 80% was investigated. In our experiments, we used ultra-clean microscope glass substrates (provided by Thermo Scientific) that were smooth, flat, and hydrophilic to the liquid drop. We used water-glycerol mixtures to vary the viscosity of the liquid and this was achieved by

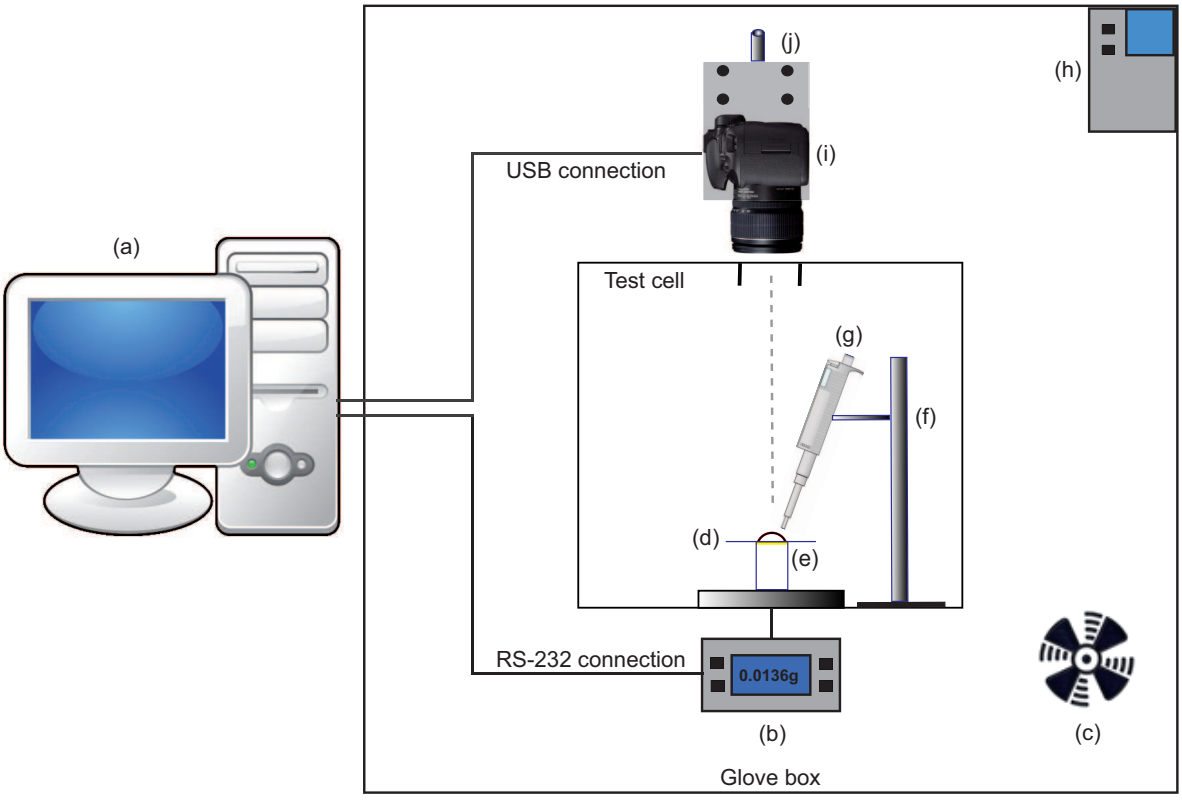

FIG. 1: Equipment used to study drop spreading dynamics: a computer **(a)**, digital balance **(b)**, fan to homogenize air inside the box (prior to the experiment) **(c)**, glass substrate **(d)**, cold back-light source **(e)**, leveling system to control the micropipette position **(f)**, digital micropipette **(g)**, humidity controller **(h)**, leveling high-precision screw to control the camera position **(j)**, and EOS 7 HD digital camera **(i)**.

increasing the amount of glycerol from 45% weight up to 74%. Using this method, the surface tension remained relatively constant, $\overline{\gamma}$ = 66.9 $\pm$ 1.5% (from 65.8 mN.m^{-1} for 74% to 68.7 mN.m^{-1} for 45% weight glycerol). This method enabled us to obtain six different viscosities ranging from 4 to 24 mPa.s. However, the calculation of the viscosity was performed using a data-driven correlations between viscosity and temperature:

$$\mu = A_1 \times T^3 + A_2 \times T^2 + A_3 \times T + A_4 \tag{1}$$

where T is in °C, and the coefficients A_1–A_4 were obtained from a polynomial fit and varied with the glycerol concentration in mass (C_m). The values of A_1–A_4 were given for some discrete concentrations, i.e., C_m = 45%, 59%, 65%, 69%, 72%, and 74%. In addition, surface tensions and density were calculated using a data-driven correlation between these two properties and temperature for different glycerol concentrations C_m:

$$\gamma = A_5 \times T + A_6 \quad \text{and} \quad \rho = A_7 \times T + A_8 \tag{2}$$

where the coefficients A_1–A_4, were obtained from a linear fit and varied with the glycerol concentration in mass. The physical properties of the various water-glycerol mixtures are summarized in Table 1. For further calculation, the exact physical properties were used. Glycerol is highly hygroscopic and therefore to neglect the variation of the viscosity over time (or the absorption process), the duration of each experiment was limited to 60 s. A pendant droplet of small controlled volume (V = 7.0 μl $\pm$ 1.0%) was slowly grown at the tip of a needle [using a digital micropipette, Fig. 1(g)] until the droplet touched the glass substrate and began to spread quasi-instantaneously. Due to the low flow rate, the approach velocity of the drop was very small and the impact velocity can be neglected. The drop was back-lit by a cold cathode light at 5000 K $\pm$ 270 K [Fig. 1(e)] to improve the image quality. The effect of the light density was studied to avoid any disturbance on the phenomenon and provided homogeneous illumination without heating the drop. Therefore, parameters of the digital camera were adjusted to the light exposure to find the best compromise between the image brightness and the edge sharpness (to improve detection of border of the liquid drop). The initial mass m_0, was recorded using a digital balance immediately just after the drop touched the glass substrate (the mass evolution was not measured). Simultaneously, the digital camera recorded the top view of the wetted area at a typical frame rate of 50 images per s (resolution of 1280 $\times$ 720 pixels) to monitor the dynamics motion of the contact line. This digital camera [Fig. 1(i)] was positioned vertically and coupled with a 1x–5x macro-lens and fixed to a leveling high-precision screw [Fig. 1(j)] to control the camera position and to minimize the vibration from the environment. Each frame of the recorded movie was processed using IMAGEJ®. The contour detection of the top-view images was performed using a circular fit of multiple points to overcome any axisymmetry problem that could occurs during the spreading dynamics. Once the contour of the droplet was detected, it was used to determine the evolution of the wetted area, $r(t)$. Additional details on our experimental setup can be found in previous articles (Bou-Zeid et al., 2013; Bou-Zeid and Brutin, 2014).

TABLE 1: Physical properties of the different water-glycerol mixtures used in the experiment

Mixture (glycerol/water)	μ **(mPa.s)**	γ **(mN.m^{-1})**	ρ **(Kg.m^{-3})**
C1 (45/55%)	4.0 $\pm$ 2.8%	68.7	1109
C2 (59/41%)	8.0 $\pm$ 2.5%	67.4	1148
C3 (65/35%)	12.1 $\pm$ 2.5%	66.8	1165
C4 (69/31%)	16.0 $\pm$ 3.1%	66.4	1175
C5 (72/28%)	20.0 $\pm$ 3.0%	66.1	1184
C6 (74/26%)	23.9 $\pm$ 2.9%	65.8	1191

3. RESULTS AND DISCUSSION

For different RH and viscosity values, we first confirmed the validity of the prediction of the hydrodynamic regime by comparing the wetting exponent of Tanner's law [$r(t) = Kt^n$, with n = 1/10] to that obtained from our experimental wetted radius as a function of time. Figure 2 shows the radius, r, of the wetted area as a function of time for a droplet of the same viscosity (μ = 12 mPa.s) and three selected humidities (RH = 30%, 40%, and 70%). We have limited our plots to three plots to ensure a clear view of the curves. For a drop of small volume (V = 7 $\mu l \pm$ 1% and $r < l_c = \sqrt{\gamma/\rho g}$ = 2.4 mm), the fluid spreads as a spherical cap shape with a circular base area at every moment in time because gravitational forces are negligible. This indicates that the instantaneous configuration of the drop can be fully described using the time-dependent base radius $r(t)$, where $r(t)$ is the wetting radius of the spreading droplet. If we try to plot the time-dependent wetted radius on a log-log scale, the obtained curve is linear (inset graph in Fig. 2), which indicates that the corresponding spreading process can be described by a power law of the form $r(t) = kt^n$, where n and k are the wetting exponent and the pre-exponential constant, respectively. However, these parameters were obtained by fitting the experimental curves on a log-log scale. For different viscosities, the wetting exponents were extracted from all of our experimental curves and plotted as a function of RH to observe a clear trend of the RH effect on the dynamics behavior (Fig. 3). In our experiments, we discarded some droplets from the analysis because they were not reproducible compared to other experiments.

Figure 3 shows the radius, r, of the wetted area as a function of time for droplets of three different viscosities (μ = 8 mPa.s, 16 mPa.s, 24 mPa.s) at 80% RH. The pre-exponential constant k was also analyzed to validate the hydrodynamic regime. According to Tanner's law, k is expected to depend linearly on $V^{3/10}(\gamma/\mu)^{1/10}$. Figures 4 and 5 show the pre-exponential constants for different viscosities and humidities. As the viscosity increases, the dynamics becomes much slower, and the pre-exponential constant k increases linearly with $V^{3/10}(\gamma/\mu)^{1/10}$. The slope of the curve extracted from the linear fit is close to the hydrodynamic regime (k = 0.84). Our observed results

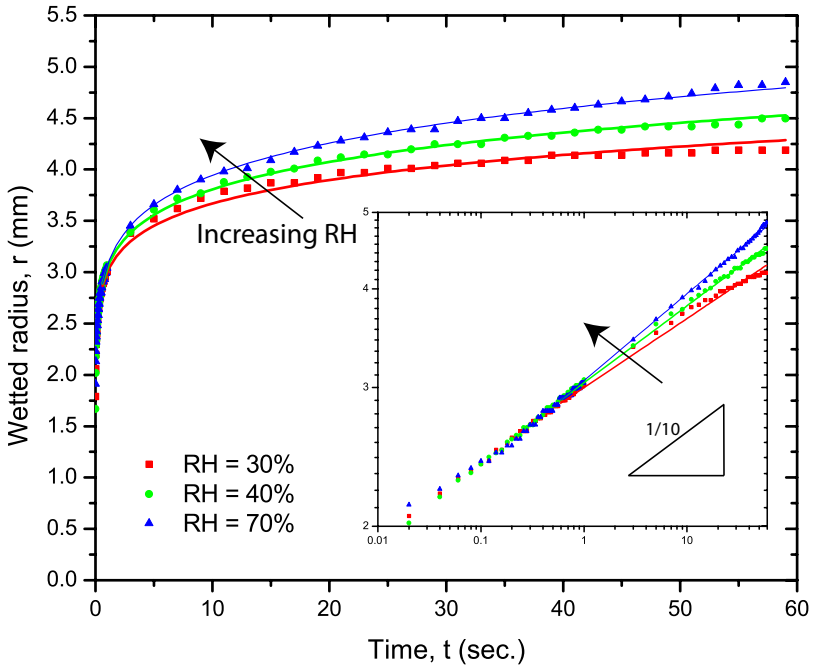

FIG. 2: The wetted radius r as function of time for three selected humidities at the same liquid viscosity (μ = 12 mPa.s). The points correspond to the experimental data, and the lines show the power fit [$r(t) = kt^n$]. The inset graph shows the experimental data on a log-log scale.

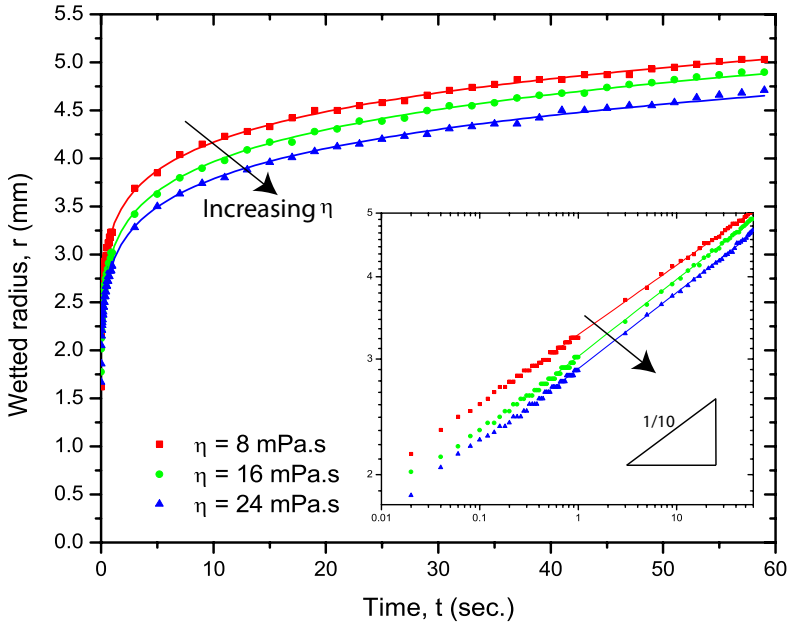

FIG. 3: Values of the fitted wetting exponent of the wetting process compared to the wetting exponent of Tanner's model (n = 0.10) (Tanner, 1979) as a function of the RH for different viscosities. The red dashed line represents the linear fit of of the wetting exponent [$n = a + b$RH with $a = 8.65 \times 10^{-2} \pm 3.31\%$, $b = 2.90 \times 10^{-2} \pm 18\%$], passing by the experimental points.

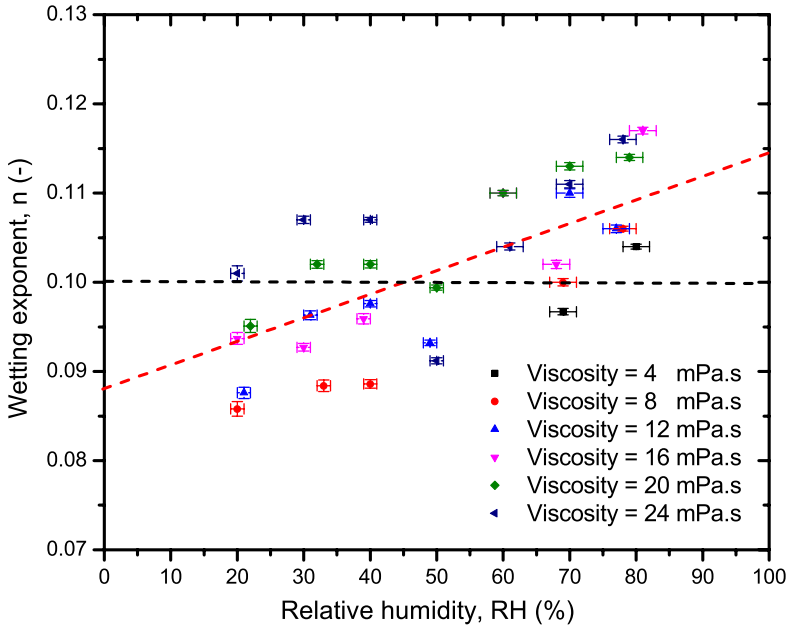

FIG. 4: The wetted radius r as function of time for three selected viscosities at same relative humidity (RH = 80%). The points correspond to the experimental data, and the lines show the power fit [$r(t) = kt^n$]. The inset graph shows the experimental data on a log-log scale.

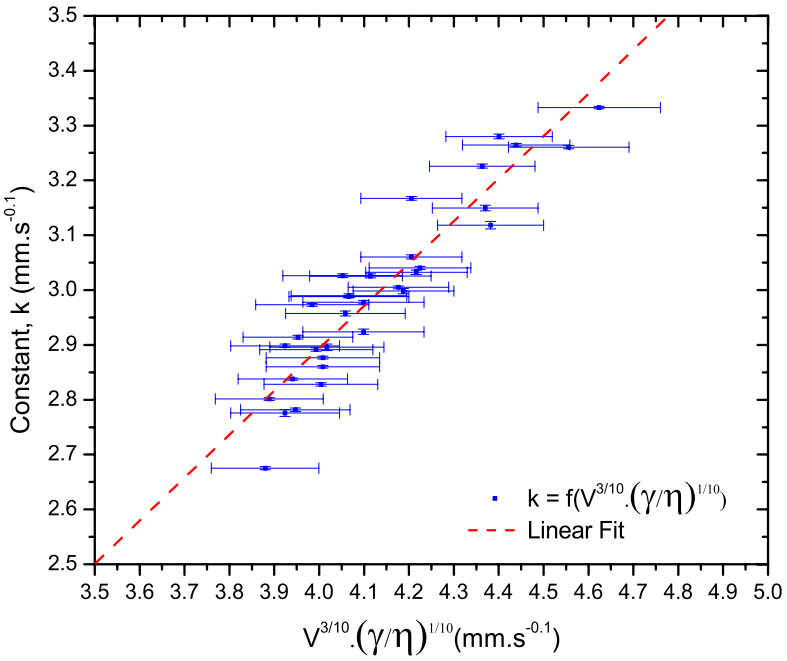

FIG. 5: Values of the fitted wetting pre-exponential constant k of the wetting process. The red dashed line is the linear fit of of the constant [$k = a + b(V^{3/10}(\gamma/\mu)^{1/10})$, where a = –0.20 $\pm$ 0.19, b = 0.77 $\pm$ 0.048], passing by the experimental points.

were consistent with the works of Eddi et al. (2013) and Roques-Carmes et al. (2010). The authors experimentally showed that the dynamics behavior decreased with viscosity and that the wetting exponent of the first and second regimes increased with viscosity. Moreover, Roques-Carmes et al. (2010) found a constant k of 0.85 $\pm$ 0.05. The authors performed experiments with droplets of different water-glycerol mixtures (V = 15 μl, μ = [20–1150] mPa.s). The authors showed that the wetting exponent corresponding to the first and second regimes increased with increasing viscosity. For small contact angles, Legendrea and Mglio (2013) observed a power law of $t^{1/2}$ and then followed by $t^{1/10}$ (Tanner's law). Their experiments revealed also an increased spreading time with increasing viscosity for liquid drops more viscous than water. In the latter case, the authors did not observe a clear evolution of Tanner's law during the final stages of spreading due to the large equilibrium contact angle. Recently, Eddi et al. (2013) studied short-time viscous droplet spreading, using a visualization that allowed accurate observation of the very early stage. The authors performed experiments with droplets of different water-glycerol mixtures on glass substrate by varying the fluid viscosity (μ = 15 mPa.s, 50 mPa.s, 220 mPa.s, 1120 mPa.s). The authors showed that the dynamics of low viscous drops was slower than high viscous drops, which is consistent with our experimental observations. Their experiments also revealed that the apparent exponent slowly decreases during the first regime, and reaches a value around 0.15. The duration of their spreading was from microseconds up to a few seconds, whereas in our experiments, the temporal resolution (50 images/s) was too small compared to their temporal resolution.

Our results revealed that the wetting exponent of the spreading process increased linearly with RH (Fig. 3). At a RH value of 46.5%, we obtained a wetting exponent of 1/10, which was consistent with the wetting exponent of Tanner's law (n = 1/10). This value of RH corresponded close to most of the RHs of experimental rooms. This can be explained by the evaporation rate occurring at the triple line, which plays an important role in the determination of the values of the wetting exponent and pre-exponential exponent. In the diffusion-controlled evaporation case, the non-uniform evaporation rate leads to temperature gradients over the drop surface (self-cooling), which leads to differences in surface tension. The region near the vicinity of the contact line is cooler than the apex because of the highest evaporation rate (Steinchen and Sefiane, 2005). As RH increases, the evaporation rate decreases at the TPCL.

The surface tension gradient could drive a Marangoni flow inside the drop that can overcome the evaporation-driven outward flow (Hu and Larson, 2006). This flow leads to a pressure gradient that drives the spreading, and the balance between the Marangoni stresses and the viscous dissipation that slows the spreading. Therefore, the Marangoni flow can give rise to additional circulation. For constant temperature, Pérez-Diaz et al. (2012) found that the water-air surface tension (pure water drops of radius R = 2.8 mm) decreases for increasing humidity in air. This effect can be considered negligible because the water-air surface tension was found to be reduced by 6% when RH was varied from 10% to 100% (T_a = 20°C).

Another possible physical mechanism could be responsible for spreading enhancement is the disjoining pressure, $\Pi(e)$, which is of comparable importance, to viscous and capillary effects (Starov and Velarde, 2009; Derjaguin et al., 1987). A very thin precursor film, referred to as an adsorbed film, can form on a solid surface in contact with vapor phase (Starov and Velarde, 2009). The disjoining pressure in this thin liquid film is defined as the excess pressure in the adsorbed film relative to that in the bulk solution and depends not only on the film thickness but also on the shape and the curvature of the interface. However, the pressure jump inside the drop is related to the curvature and to the disjoining pressure. As RH increases, the vapor pressure in the air increases. Thus, a decrease in RH would affect the curvature of the meniscus and thus, enhance the disjoining pressure. Thus, enhanced spreading can be observed with RH corresponding to increased values of the wetting exponent. In contrast to these observed results, we have shown that the spreading rate is enhanced due to the evaporation rate at the TPCL in the case of complex fluids (whole blood) (Bou-Zeid and Brutin, 2014). In this work, a wetting exponent of 0.19 was found in the case of drops of blood (second-low spreading regime). This was because whole blood is a complex suspension in which the biocolloids play an important role in pinning the contact line and interaction between particles and the glass substrate. The increased meniscus curvature near the TPCL of an advancing wetting front could lead to condensation, which contributes to the overall spreading (Shanahan, 2001). However, there must be an additional contribution from the evaporation rate that can affect the internal flow and the interfacial liquid-vapor surface tension. When a drop touches the hydrophilic surface, the drop spreads over the substrate to minimize the total surface energy. For small drops whose radii are smaller than the capillary length, the effects of gravity are negligible and spreading is driven by capillary forces. Consequently, capillary forces dominate the flow motion inside the droplets. At a very early time of spreading, the surface of the drop significantly deforms as a capillary flow travels along the surface of the drop. In this case, capillary forces rapidly drive spreading due to the curved surface, whereas the viscous forces of the fluid resist deformation. Once the capillary flow has dissipated, the droplets spreads at a slower rate.

4. CONCLUSIONS

The effect of RH on the dynamics of drop spreading on a clean glass surfaces was investigated. Our experiments demonstrated that the evolution of the wetted radius is described by a similar law to the Tanner's law: $r(t) = kt^n$ with k and n function of the room humidity and the fluid viscosity. We showed that, beyond Tanner's law, there is an updated spreading coefficient that takes into account the room humidity. The updated model is in the form: $r(t) = kt^n$, where n = 0.0865 + 0.0290 RH. For RH = 46.5%, Tanner's model is quantitatively correct. The enhanced spreading rate can be explained by the evaporation rate at the triple line. However, this important result requires further validation for other mixtures to generalize the spreading coefficient (n). For other fluids, the same analysis can be performed to take into account the triple line evaporation as a function of the vapor concentration.

REFERENCES

Ajaev, V. S., Gambaryan-Roisman, T., and Stephan, P., Static and dynamic contact angles of evaporating liquids on heated surfaces, *J. Colloid Interface Sci.*, vol. **342**, p. 550, 2010.

Anderson, D. M. and Davis, S. H., The spreading of volatile liquid droplets on heated surfaces, *Phys. Fluids*, vol. **7**, p. 248, 1995.

Attinger, D., Zhao, Z., and Poulikakos, D., Experimental study of molten microdroplet surface deposition and solidifcation: Transient behavior and wetting angle dynamics, *Heat Mass Transfer*, vol. **122**, pp. 544–546, 2000.

Bonn, D., Eggers, J., Indekeu, J., Meunier, J., and Rolley, E., Wetting and spreading, *Rev. Mod. Phys.*, vol. **81**, pp. 739–805, 2009.

Bou-Zeid, W. and Brutin, D., Effect of relative humidity on the spreading dynamics of sessile drops of blood, *Colloids Surf. A*, vol. **456**, pp. 273–285, 2014.

Bou-Zeid, W., Vicente, J., and Brutin, D., Influence of evaporation rate on cracks formation of a drying drop of whole blood, *Colloids Surf. A*, vol. **432**, no. 2, pp. 139–146, 2013.

Cazabat, A. M. and Cohen Stuart, M. A., Dynamics of wettlng: Effects of surface roughness, *J. Phys. Chem.*, vol. **90**, pp. 5845–5849, 1986.

Chhasatia, V. H., Joshi, A. S., and Sun, Y., Effect of relative humidity on contact angle and particle deposition morphology of an evaporating colloidal drop, *Appl. Phys. Lett.*, vol. **97**, p. 231909, 2010.

Cox, R. G., The dynamics of the spreading of liquids on a solid surface, *J. Fluid Mech.*, vol. **168**, pp. 195–220, 1986.

Derjaguin, B. V., Churaev, N. V., and Muller, V. M., Surface forces, *Plenum Press*, 1987.

Duvivier, D., Seveno, D., Rioboo, R., Blake, T. D., and De Coninck, J., Experimental evidence of the role of viscosity in the molecular kinetic theory of dynamic wetting, *Phys. Rev. E*, vol. **27**, pp. 13015–13021, 2011.

Eddi, A., Winkels, K. G., and Snoeijer, J. H., Short time dynamics of viscous drop spreading, *Phys. Fluids*, vol. **25**, p. 013102, 2013.

Ehrhard, P., Experiments on isothermal and nonisothermal spreading, *J. Fluid Mech.*, vol. **257**, pp. 463–483, 1993.

de Gennes, P. G., Wetting: statics and dynamics, *Rev. Mod. Phys.*, vol. **57**, p. 827, 1985.

Hu, H. and Larson, R. G., Marangoni effect reverses coffee-ring depositions, *J. Phys. Chem. B.*, vol. **110**, pp. 7090–7094, 2006.

Pérez-Diaz, J. L., Alvarez-Valenzuela, A. M., and Garcia-Prada, C. J., The effect of the partial pressure of water vapor on the surface tension of the liquid water-air interface, *J. Colloid Interface Sci.*, vol. **181**, pp. 180–182, 2012.

Legendre, D. and Maglio, M., Numerical simulation of spreading drops, *Colloids Surfaces A*, vol. **432**, pp. 29–37, 2013.

Lopez, J., Miller, C. A., and Ruckenstein, E., Spreading kinetics of liquid-drops on solids, *J. Colloid Interface Sci.*, vol. **56**, pp. 4660–4468, 1971.

Roques-Carmes, T., Mathieu, V., and Gigante, A., Experimental contribution to the understanding of the dynamics of spreading of newtonian uids: Effect of volume, viscosity and surfactant, *J. Colloid Interface Sci.*, vol. **344**, pp. 180–197, 2010.

de Ruijter, M. J., De Coninck, J., and Oshanin, G., Droplet spreading: Partial wetting regime, *Langmuir*, vol. **15**, pp. 2209–2216, 1999.

Shanahan, M. E. R., Condensation transport in dynamic wetting, *Langmuir*, vol. **17**, pp. 3997–4002, 2001.

Starov, V. M. and Velarde, M. G., Surface forces and wetting phenomena, *J. Phys.: Condens. Matter*, vol. **21**, p. 464121, 2009.

Steinchen, A. and Sefiane, K., Self-organised marangoni motion at evaporating drops or in capillary menisci, *J. Non-Equilib. Thermodyn.*, vol. **30**, pp. 39–51, 2005.

Tanner, L., The spreading of silicone oil drops on horizontal surfaces, *J. Phys. D: Appl. Phys.*, vol. **12**, pp. 1473–1484, 1979.